Supporting Information

Hu et al. 10.1073/pnas.1009219107

SI Text

Multispin Analysis of NMR Distance Measurements.

$^{13}C\{^{31}P\}$REDOR analysis of citrate distances from apatite. $^{13}C\{^{31}P\}$ dipolar coupling measurements by $^{13}C\{^{31}P\}$REDOR NMR can provide insights into the distances of various citrate carbons from the apatite surface. Fig. 3 *A* and *B* shows $^{13}C\{^{31}P\}$ REDOR data for all five spectrally resolved carbon sites in citrate bound to apatite in bone. While many systems studied by REDOR can be approximated in terms of two or few interacting spins, a ^{13}C spin near an apatite surface experiences the dipolar fields of many ^{31}P nuclear magnets. The initial decay depends on the second moment of the ^{13}C-^{31}P couplings

$$M_2 = \Sigma_n \omega^2_{C\text{-}P,n} = \Sigma_n C_n(\alpha,\beta,\gamma) 1/r^6_{C\text{-}P,n},$$

where $r_{C\text{-}P,n}$ is the distance between the carbon and the nth ^{31}P spin, and $C_n(\alpha,\beta,\gamma)$ is a purely orientation-dependent prefactor. At sufficiently large distances of the ^{13}C from the apatite surface ($z_{C\text{-}P} > 1$ nm), the second moment depends only on the height $z_{C\text{-}P}$ above the top phosphate layer, independent of the lateral (x-y) position of the ^{13}C. However, when the height $z_{C\text{-}P}$ is not much larger than the average P-P distance of 0.45 nm in apatite, the x-y position of the ^{13}C spin needs to be taken into account. Fig. S1*A* shows a contour plot of the distance-only heteronuclear second moment

$$M_{2r} = \Sigma_n 1/r^6_{C\text{-}P,n}$$

as a function of ^{13}C position at a fixed height of $z_{C\text{-}P} = 0.35$ nm above a $(10\bar{1}0)_1$ hydroxyapatite surface. The plot shows pronounced maxima above ^{31}P (of slightly different height for two types of phosphate at different depths from the apatite surface) and wide flat regions around the Ca ions. Negatively charged citrate is expected to be repelled by the negatively charged phosphate and rather bound to calcium. Therefore, the regions of high M_{2r} near ^{31}P can mostly be disregarded. In addition, the regions of high M_{2r} account for only a small fraction of the total area, see the histogram of M_{2r} in Fig. S1*B*. Calcium ions are located 0.05 nm below the top phosphate layer, so $z_{C\text{-}Ca} = z_{C\text{-}P} + 0.05$ nm.

Fig. S1*C* shows simulated REDOR curves and data from Fig. 3*B* for the 15 positions B1–B5, C1–C5, and D1–D5 marked in Fig. S1*A* and $z_{C\text{-}P}$ values between 0.3 and 0.5 nm. The height of the ^{13}C nucleus above calcium is larger by 0.05 nm. The data of Fig. 3 show that the central and one terminal COO group are closest to the surface, while the other terminal carboxylate is at a 0.1-nm greater height but still close to apatite. In the simulations of the REDOR curves, the second moment with REDOR angular dependencies of all the ^{31}P-^{13}C couplings was calculated for >3,000 crystallite orientations, via orientational averaging of the rotor-axis relative to the crystallite normal, and rotation of the B_0 field around the rotor-axis (with the fixed magic angle between them), as outlined in ref. 1. The total dephasing curve is a superposition, for various rotor-axis and B_0-field orientations, of Gaussians $\exp(-M_2(Nt_r)^2/2)$, with the second moment M_2 evaluated based on the internuclear distances and the REDOR angular dependences of the individual C-P couplings at the given rotor-axis and B_0 orientation. The simulation program was validated using a spin-pair model geometry.

Calculation of the citrate density on bone mineral. The area density of citrate on apatite in bone and bound to bone mineral can be calculated from the known structural parameters of the materials. The 3-nm thick nanocrystals in bone, alternating with 3-nm thick collagen layers, have a surface-to-sample-volume ratio of

$$S/V_{\text{bone}} = 2\ \text{A}/[(3+3)\ \text{nm A}] = 0.33/\text{nm} = 0.33 \times 10^9/\text{m}$$

and the nanocomposite has an average density of

$$\begin{aligned}\rho_{\text{ave}} &= m_{\text{bone}}/V_{\text{bone}} = (\rho_A V_A + \rho_B V_B)/V_{\text{bone}} \\ &= \rho_A V_A/V_{\text{bone}} + \rho_B V_B/V_{\text{bone}} = (1.15 + 3.2)\text{g/cm}^3 \times 0.5 \\ &= 2.2\ \text{g/cm}^3 = 2.2 \times 10^6\ \text{g/m}^3\end{aligned}$$

calculated from 50:50 volume fractions and densities of collagen (1.15 g/cm^3) and apatite (3.2 g/cm^3). From these quantities, the specific surface area (per mass) of bone can be calculated as

$$\begin{aligned}S/m_{\text{tot}} &= (S/V_{\text{tot}})/(m_{\text{tot}}/V_{\text{tot}}) = (S/V_{\text{tot}})/\rho_{\text{ave}} \\ &= 0.33 \times 10^9/\text{m}/(2.2 \times 10^6\ \text{g/m}^3) = 150\ \text{m}^2/\text{g} \\ &= 150 \times 10^{18}\ \text{nm}^2/(\text{g bone}).\end{aligned}$$

Also, according to wet chemistry and our spectroscopic analysis, 1 g of bone contains 1.2 wt% = 12 mg citrate, which corresponds to 0.012 g/189 g/mol = 6.3×10^{-5} mol of citrate per g of bone, or $n_{\text{citr}}/m_{\text{tot}} = 6.3 \times 10^{-5} \times 6 \times 10^{23} = 3.8 \times 10^{19}$ citrate molecules/(g bone). The area density is thus

$$\begin{aligned}(n_{\text{citr}}/m_{\text{tot}})/(S/m_{\text{tot}}) &= 3.8 \times 10^{19}/(150 \times 10^{18}\ \text{nm}^2) \\ &= 0.25/\text{nm}^2 = 1/(2\ \text{nm})^2\end{aligned}$$

The density of ^{13}C-labeled citrate on the NuOss™ bone mineral, with a measured specific surface area of

$$S/m_{\text{tot}} = 60\ \text{m}^2/\text{g}$$

can be calculated from the 0.8 mg of citrate, determined by NMR calibrated on neat citrate, per 0.19 g of bone mineral in the same sample. The total bone-mineral surface area in that sample is

$$\begin{aligned}S &= (S/m_{\text{tot}})m_{\text{tot}} = 60\ \text{m}^2/\text{g} \times 0.19\ \text{g} = 11.4\ \text{m}^2 \\ &= 11.4 \times 10^{18}\ \text{nm}^2.\end{aligned}$$

The 0.8 mg of citrate correspond to 0.0008 g/189 g/mol = 4.2×10^{-6} mol and thus $n_{\text{citr}} = 4.2 \times 10^{-6} \times 6 \times 10^{23} = 2.54 \times 10^{18}$ citrate molecules. The area density of citrate on bone mineral is thus

$$n_{\text{citr}}/S = 2.54 \times 10^{18}/11.4 \times 10^{18}\ \text{nm}^2 = 0.22/\text{nm}^2 = 1/(2\ \text{nm})^2$$

in good agreement with the value for bone obtained above.

CODEX ^{13}C NMR simulations. The CODEX NMR data of citrate with ^{13}C-labeled terminal COO^- groups shown in Fig. 4 were fitted by simulating the spin exchange between 600 ^{13}C spins in half as many citrate molecules, distributed on a flat rectangular surface of 10 nm width and *ca*. 100 nm length. The spin exchange

is characterized by an exchange matrix Π, with off-diagonal elements

$$\Pi_{\mathrm{nm}} = 0.5\pi[2\pi 7.5\ \mathrm{kHz}\, 10^{-3}\ \mathrm{nm}^3/r_{\mathrm{nm}}{}^3]^2\langle(P_2(\cos\theta))^2\rangle F(0)$$

reflecting the coupling between ^{13}C spins n and m. The value of F(0) = 0.025ms is calibrated by matching the initial decay due to the 0.5-nm intramolecular spin-pair coupling, and is close to literature values for ^{13}COO groups between 0.025 and 0.044 ms (2). The diagonal element Π_{nn} is the negative of the sum of the nth column of off-diagonal elements.

The pointed brackets of $\langle(P_2(\cos\theta))^2\rangle$ indicate the time averaging, due to magic-angle spinning, of the orientation dependence of the dipolar interaction, which depends on the instantaneous angle θ between the C^n-C^m internuclear vector and the external B_0 field. This average depends on the angle β between the internuclear vector and the rotor-axis. Rather than using only the β-averaged value (0.2) of $\langle(P_2(\cos\theta))^2\rangle$, we calculated $\langle(P_2(\cos\theta))^2\rangle$ as a function of cosβ numerically and took the variation of $\langle(P_2(\cos\theta))^2\rangle$ into account by selecting a random value of cosβ between −1 and +1 for each internuclear vector r_{nm} and using the corresponding value of $\langle(P_2(\cos\theta))^2\rangle$ in the calculated value of Π_{nm} according to the equation above. This approach provides the same variation of the squared coupling frequencies as full powder averaging and reproduces the observed nonexponential decays (2) better than simulations with a fixed value of $\langle(P_2(\cos\theta))^2\rangle$.

The normalized CODEX signal $S_{\mathrm{CODEX}}(t)$, which is the fraction of the magnetization remaining on the spin on which it started out, averaged over all spins, is calculated from the standard solution for the N-component vector $\mathbf{M}$ of the z-magnetization values of the N exchanging spins

$$\mathbf{M}(t) = \exp(\Pi t)\mathbf{M}(0)$$

as

$$S_{\mathrm{CODEX}}(t) = \sum_{n=1}^{N}(\exp(\Pi t)\mathbf{e}_n)_n = \mathrm{tr}(\exp(\Pi t)).$$

In the intermediate step, $\mathbf{e}_n$ is the unit vector with elements $(\mathbf{e}_n)_m = \delta_{\mathrm{nm}}$ (i.e., 1 for $n = m$ and 0 otherwise), representing an initial state $\mathbf{M}(0) = \mathbf{e}_n$ with magnetization only on spin n. For a sufficiently long dephasing and refocusing time Nt_r, the detected CODEX signal from that spin is proportional to the magnetization $M_n(t) = (\exp(\Pi t)\mathbf{e}_n)_n$ remaining on that same spin n. The sum over n provides the summation of the contributions from all N ^{13}C spins; the trace operation (sum of diagonal elements) on the right-hand side of the equation achieves this in a particularly convenient way.

The simulated CODEX curves depend on the density and positional ordering of the citrate molecules. The ^{13}C distributions corresponding to the seven fit curves in Fig. 4 are displayed in Fig. S2. Partial positional ordering is achieved by increasing the excluded area around the center of each molecule. Minimal ("random") ordering is generated by an excluded-area diameter of $d_{\mathrm{excl}} = 0.8$ nm that corresponds to the diameter of a citrate molecule. For an area density of $1/d_{\mathrm{cc}}{}^2$ moderate ordering was obtained with $d_{\mathrm{excl}} = 0.6\ d_{\mathrm{cc}}$, and partial ordering with $d_{\mathrm{excl}} = 0.75\ d_{\mathrm{cc}}$. A higher than average ($>1/(2\ \mathrm{nm})^2$) citrate density is possible for the citrate-covered apatite surfaces, if other surfaces have little or no citrate bound. For instance, the average density of $1/(2\ \mathrm{nm})^2$ can be obtained by combining 50% of surfaces at $1/(1.4\ \mathrm{nm})^2$ (which yield signal) and 50% of surfaces without any citrate (which do not contribute to the measured signal).

1. Schmidt-Rohr K, Rawal A, Fang XW (2007) A new NMR method for determining the particle thickness in nanocomposites, using T_{2H}-selective $X\{^1\mathrm{H}\}$ recoupling. *J. Chem. Phys* 126:054701/054701–054716.

2. Luo W, Hong M (2006) Determination of the oligomeric number and intermolecular distances of membrane protein assemblies by anisotropic H-1-driven spin diffusion NMR spectroscopy. *J. Am. Chem. Soc* 128:7242–7251.

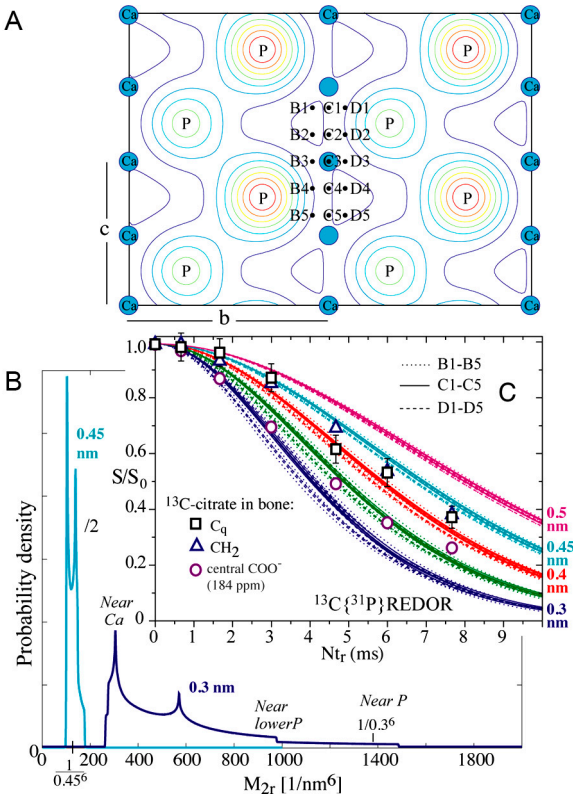

Fig. S1. Analysis of parameters in $^{13}C\{^{31}P\}$ REDOR simulations for citrate carbons in bone. (*A*) Contour plot of the distance-only second moment M_{2r}, i.e., essentially the sum of the squares of the ^{13}C-^{31}P dipolar couplings, calculated as a function of ^{13}C position at a fixed height $z_{C\text{-}P} = 0.3$ nm above the top phosphate layer in apatite. Apart from pronounced maxima above the P atoms, wide areas with similar dipolar couplings are seen, in particular surrounding the calcium atoms (light blue circles). Likely positions of the five carbons in citrate, spaced by the projected C-C distance of 0.125 nm in an all-trans chain, are indicated along the c-axis as C1–C5. Corresponding positions laterally displaced by 0.1 nm are marked B1–B5 and D1–D5. (*B*) Corresponding "histogram" of distance-only second moments M_{2r}. The large M_{2r} values corresponding to positions above P are seen to be rare. The narrower histogram for a 0.45-nm height above the top phosphorus layer is also shown. (*C*) Data points of exchanged ^{13}C-labeled citrate in bone (symbols as in Fig. 3*B*) and simulated REDOR dephasing curves for the fifteen points marked B1—D5 in A) at the indicated $z_{C\text{-}P}$ heights of ^{13}C above the top phosphorus layer. C1–C5: full lines; B1–B5: dotted lines; and D1–D5: dashed lines.

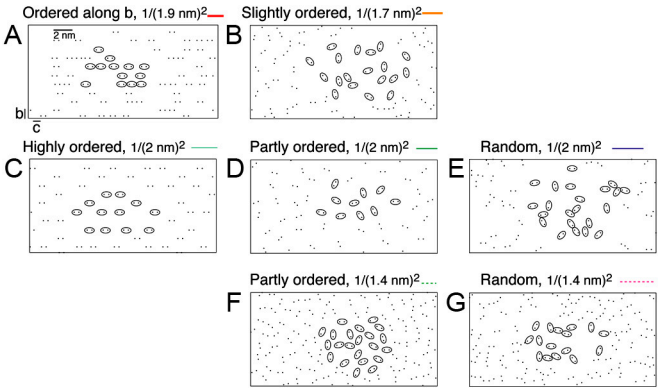

Fig. S2. Distributions of terminal-^{13}COO groups of citrate (each ^{13}C is marked as a black dot, and some molecules are indicated by elliptical outlines) for the seven fit curves in Fig. 4. (*A*) Best fit, for an area density of $1/(1.9\text{ nm})^2$ and positional ordering in one dimension. (*B*) Best fit, for an area density of $1/(1.7\text{ nm})^2$ and slight positional ordering. (*C*) Distribution corresponding to a curve above the experimental data, for $1/(2\text{ nm})^2$ and significant positional ordering. (*D*) Distribution corresponding to a curve below the experimental data, for $1/(2\text{ nm})^2$ and partial positional ordering. (*E*) Distribution corresponding to a good fit, for $1/(2\text{ nm})^2$ and minimal positional ordering ("random"). (*F*) Distribution corresponding to a curve slightly below the experimental data, for $1/(1.4\text{ nm})^2$ and partial positional ordering. (*G*) Distribution corresponding to a curve below the experimental data, for $1/(1.4\text{ nm})^2$ and minimal positional ordering.